Engineering Structures 231 (2021) 111650

Contents lists available at ScienceDirect

Engineering Structures

journal homepage: www.elsevier.com/locate/engstruct

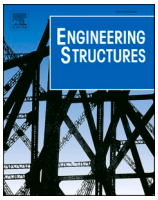

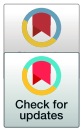

The influence of the kinematics of rough surface engagement on the transfer of forces in cracked concrete

Miguel Fernández Ruiz

Ecole Polytechnique Fédérale de Lausanne, School of Architecture, Civil and Environmental Engineering, Lausanne, Switzerland

ARTICLE INFO

Keywords:
Aggregate interlock
Concrete
Limit analysis
Crack disengagement
Localized cracking
Smeared cracking

ABSTRACT

One of the most instrumental aspects governing the response of structural concrete at ultimate limit state refers to the possibility of developing smeared cracking patterns within a member (associated normally to the presence of sufficient reinforcement for control of cracking) or whether failures are associated to localization of strains in a single crack. In the former case, the strains are smeared. New cracks can develop at different orientations and stress redistributions occur in a controlled manner. These cases are governed by equilibrium and by material yield conditions and can thus be designed according to limit analysis. The response corresponding to crack localization is however associated to potentially brittle failures, occurring by a sudden opening and sliding of a critical crack, and does not normally allow for controlled redistributions of stresses. In this case, the shape and kinematics of the critical crack are governing for the strength of the member and design methods based on limit analysis are generally not applicable.

In this paper, a discussion on the transfer of forces in cracked concrete is presented, allowing to consider in a consistent manner both cases where smeared or localized cracking occur. This is investigated by means of the stress state developed in the vicinity of a localized crack and accounting for equilibrium, kinematics and material damage conditions. The approach presented allows for a comprehensive view of the phenomenon of transfer of forces through cracked concrete and to describe cases governed by the material strength or by friction conditions depending on the crack kinematics. On this basis, the implications for shear design of concrete members are discussed.

1. Introduction

Traditionally, the design of reinforced concrete members at ultimate limit state has been performed based on different approaches depending on the presence or not of a reinforcement for crack control. Without such reinforcement, cracks can propagate in an uncontrolled manner localizing the strains. The width of the cracks under these conditions can be relatively high and limit the potential capacity to transfer forces through them by aggregate interlocking or by the residual tensile strength of concrete [1]. This situation may eventually lead to brittle failures by disengagement (separation) of the crack lips. On the contrary, when sufficient reinforcement crossing the cracks is arranged, the cracks develop in a controlled manner. This is associated to the activation of the reinforcement and to the development of new cracks, which limit the crack spacing and their opening (smearing thus the strains and avoiding localization issues).

A detailed view of this issue is presented in Fig. 1a,b, showing the cracking pattern of two nominally identical specimens tested by Yoon et al. [2], where one (H1-S, Fig. 1a) does not have transverse reinforcement while the other (H2-N, Fig. 1b) has a fairly high amount of transverse reinforcement ($\rho_w = 0.23\%$). In the first specimen, a number of bending cracks develop and progress. These cracks, within the shear span, develop first quasi-vertically (inclined according to the level of shear force [1,3]) up to the location of the neutral axis. For higher levels of load, they develop a second, quasi-horizontal, branch [1]. As it can be seen (Fig. 1a), these cracks may merge, leading to the development of a critical shear crack localizing the strains [4]. Such crack has a significantly higher crack opening than the others, governing the strength of the member and eventually leading to failure [1,3] by disengagement of its lips.

A detail of the typical kinematics of the critical shear crack in case no reinforcement for crack control is arranged is shown in Fig. 1c (corresponding to specimen SC65 tested by Cavagnis et al. [1] on a similar geometry as the tests by Yoon et al. and where the displacement field was tracked by means of Digital Image Correlation techniques). As it can be seen from the relative displacement of the critical shear crack, the crack opens according to the location of the centre of rotation defining

E-mail address: miguel.fernandezruiz@epfl.ch.

https://doi.org/10.1016/j.engstruct.2020.111650
Received 9 July 2020; Received in revised form 27 October 2020; Accepted 26 November 2020
Available online 20 January 2021

Nomenclature

a	Shear span
c	Depth of the compression zone
d	Effective depth
d_g	Maximum aggregate size
d_{g0}	Reference size
f_R	Resistance
f_c	Concrete strength in compression measured in cylinder
f_{c0}	Reference concrete strength
f_{cp}	Equivalent plastic strength
n	Normal coordinate
r	Roughness
s	Crack spacing
t	Tangential coordinate
$\dot{u}$	Incremental displacement
w	Crack opening
w_0	Initial crack opening
x_A	Distance characterizing the location of the critical shear crack
M	Acting bending moment
N	Normal force
V	Applied shear force
α	Angle of crack displacement (with respect to crack plane)
α_t	Tangent angle of crack displacement (with respect to crack plane)
β	Angle of yield line
δ	Crack slip
ε	Strain
$\dot{\varepsilon}$	Increment of strain
φ	Friction angle of concrete
ϕ	Dilatancy angle
γ	Shear strain
η_{fc}	Efficiency factor for concrete brittleness
η_w	Efficiency factor for concentrated crack opening
η_{is}	Efficiency factor for casting conditions
η_D	Efficiency factor for duct disturbances
η_ε	Efficiency factor for smeared crack opening
μ	Friction angle
ω	Mechanical reinforcement ratio
θ	Angle of stress field
ρ	Reinforcement ratio
ρ_w	Transverse reinforcement ratio
σ	Stress
σ_n	Normal stress
σ_t	Tangential stress
τ	Shear stress
ψ	Rotation
ζ	Width of plastic band

the local kinematics. Such centre, for members without transverse reinforcement, is approximatively located at the tip of the critical shear crack [5] and moves gradually towards the load introduction plate as the length of this crack progresses [3]. As a result of this process, this crack opens at every point (component w in Fig. 1c) but also slides in its quasi-vertical region (component δ in Fig. 1c), allowing to transfer forces by aggregate interlocking (the potential role of other shear-carrying actions is thoroughly described elsewhere [3,5]). It shall be noted that for increasing levels of load (increasing the demand of shear force to be transferred), the critical shear crack also increases its opening, which is detrimental for the capacity to transfer shear stresses across cracked concrete [5,6,7]. Thus, when the shear demand equals the capacity of cracked concrete, failure occurs by a sudden disengagement of the critical shear crack lips (leading to their separation and sliding, refer to grey vertical vectors in Fig. 1c) and is associated to a decay in the capacity of the potential shear-transfer actions [8].

When sufficient transverse reinforcement is arranged (as for specimen H2-N, see Fig. 1b), the crack pattern is notably different. The width of the primary cracks remains controlled and new cracks may develop. Such new cracks originate in most cases from the primary cracks and have usually a rotated (flatter) inclination than them (refer to Fig. 1b). As a consequence of the higher number of cracks and that their spacing remains limited, the opening of the cracks is low, ensuring a high capacity to transfer compressive stresses [9,10,11]. The load can thus be transferred by compression fields (developing in the cracked concrete) in equilibrium with tension ties (developing at the transverse reinforcement) [12]. The shear resistance is consequently not governed by the formation of a critical shear crack localizing the strains (no such a crack was for instance reported in specimen H2-N in Fig. 1b), but by the yielding of the stirrups and by the crushing capacity of concrete (softened by the presence of the cracks locally disturbing the transfer of forces with respect to an uncracked situation [9]).

From the previous observations, it can be highlighted the fundamental difference in the response of members with and without control of cracking. In the latter case, a critical crack localizes the strains, limiting the capacity to transfer forces and potentially triggering failure by crack disengagement (provided that other load-carrying actions cannot ensure the transfer of forces [13,14]), see Fig. 2a. On the contrary, when the cracks have limited width (typically associated to the presence of a reinforcement for crack control), high contact forces can develop between rough surfaces, allowing for a potential development of secondary (smeared) cracking at a rotated angle, see Fig. 2b.

In this paper, the phenomenon of the transfer of forces through rough cracked surfaces is investigated by means of a physical approach combining the principles of limit analysis and material damage. This approach provides a consistent basis to describe the phenomenon and allows for a smooth transition between the development of smeared and localized cracking conditions (Fig. 2). It can additionally be used to characterize the development of stresses (normal and tangential) as a function of the acting kinematics (crack opening and sliding). The results are validated on the basis of a large experimental database and by comparison to selected tests, aimed both at low and high crack opening conditions and with different failure modes. Finally, the implications of this approach are discussed with reference to the response of beams in shear.

In order to present the ideas of this paper in a transparent manner, a review of some concepts from limit analysis is presented in Section 2 and Appendix A. This review is not intended as a repetition of the state-of-the-art, but it is elaborated from an original perspective, merging the analysis of mechanisms with the concepts of the equilibrium of stresses at a yield line or plastic band.

2. The concept of plastic band and yield line according to limit analysis

The transfer of forces in presence of discontinuities can be efficiently described within the frame of limit analysis [15]. In the following, this will be performed by considering that deformations concentrate within a plastic band with thickness ζ, see Fig. 3a. The kinematics of this region corresponds to a linearly increasing increment of displacement ($\dot{u}$) at an angle α (Jensen [16]):

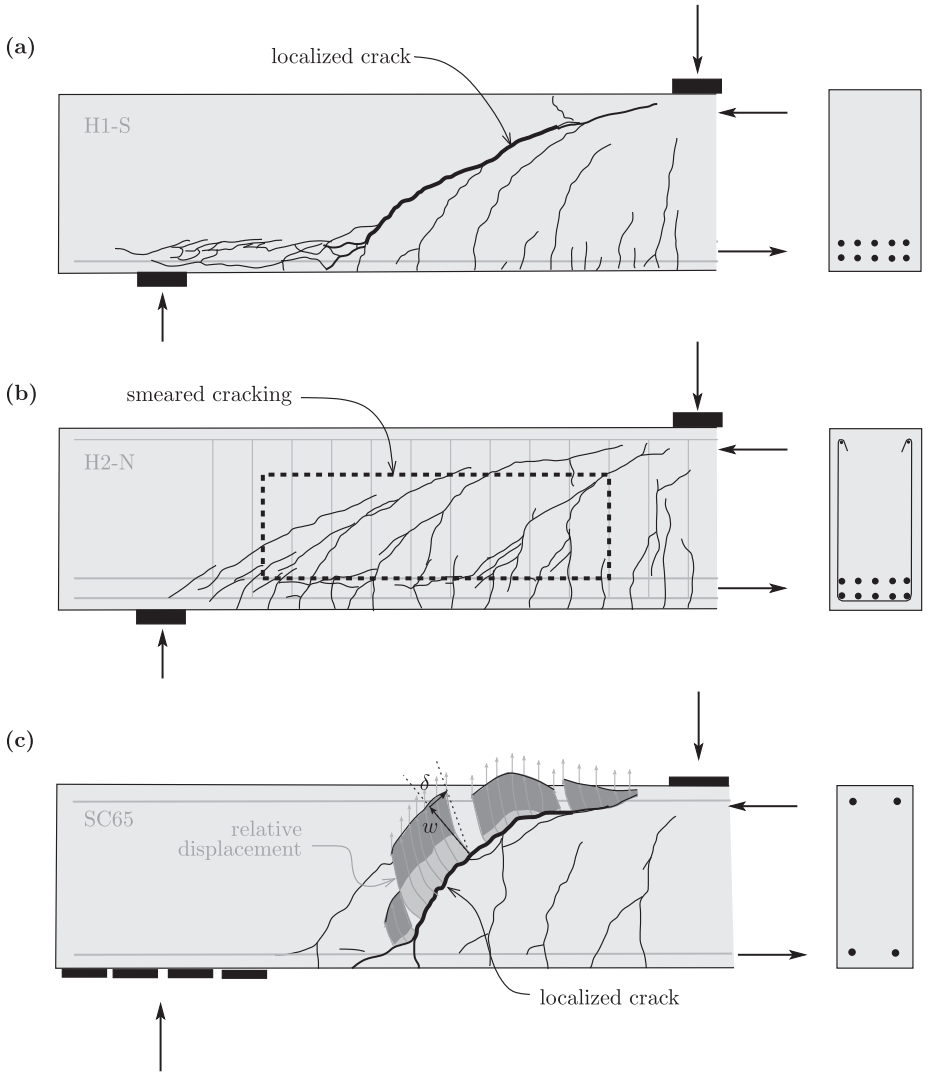

Fig. 1. Development of cracking in members subjected to shear and bending: (a) cracking pattern of specimen H1-S by Yoon et al [2]; (b) cracking pattern of specimen H2-N by Yoon et al [2]; and (c) cracking pattern and kinematics of specimen SC65 by Cavagnis et al. [1]

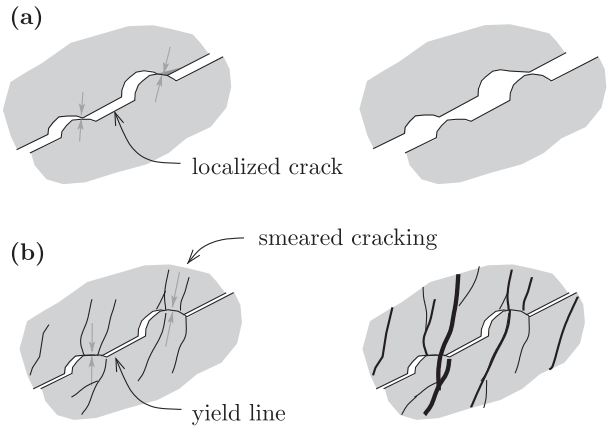

Fig. 2. Transfer of forces through a rough surface: (a) case of large crack openings and surface sliding; and (b) case of low crack openings and development of smeared cracking.

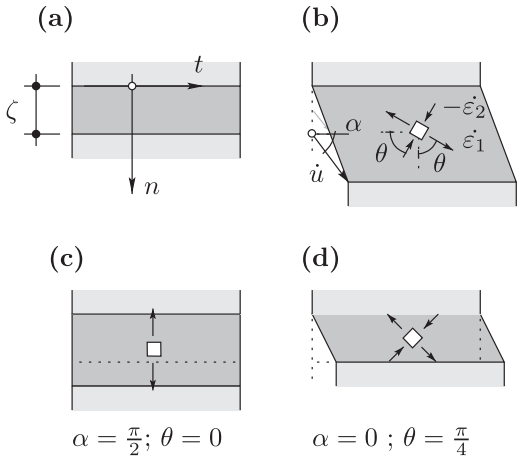

Fig. 3. Plastic band: (a) geometry and axes; (b) displacement and strain fields; (c) case of pure separation; and (d) case of pure shearing.

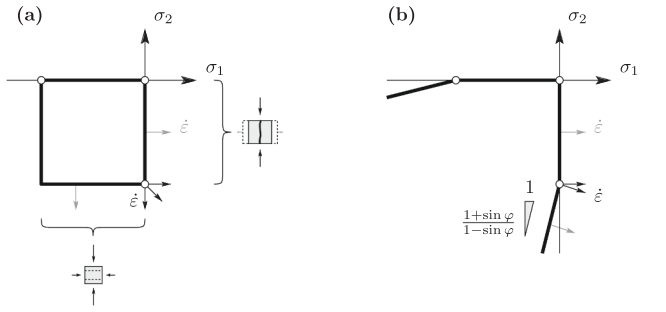

Fig. 4. Mohr-Coulomb yield surfaces (with tension cut-off): (a) plane stress conditions; and (b) plane strain conditions.

$$\begin{aligned}\dot{u}_n &= \frac{n}{\zeta}\dot{u}sin\alpha \\ \dot{u}_t &= \frac{n}{\zeta}\dot{u}cos\alpha\end{aligned} \tag{1}$$

The strain field can be directly derived from the displacement field as follows:

$$\begin{aligned}\dot{\varepsilon}_t &= \frac{\partial \dot{u}_t}{\partial t} = 0 \\ \dot{\varepsilon}_n &= \frac{\partial \dot{u}_n}{\partial n} = \frac{\dot{u}}{\zeta}sin\alpha \\ \dot{\gamma}_{nt} &= \frac{\partial \dot{u}_t}{\partial n} + \frac{\partial \dot{u}_n}{\partial t} = \frac{\dot{u}}{\zeta}cos\alpha\end{aligned} \tag{2}$$

whose principal strain increments and directions result (Fig. 3b):

$$\begin{aligned}\theta &= \frac{\pi}{4} - \frac{\alpha}{2} \\ \dot{\varepsilon}_1 &= \frac{1}{2}\frac{\dot{u}}{\zeta}(sin\alpha + 1) \\ \dot{\varepsilon}_2 &= \frac{1}{2}\frac{\dot{u}}{\zeta}(sin\alpha - 1)\end{aligned} \tag{3}$$

As it can be noted, this simple shape and kinematics allows reproducing a number of strain increment fields, as pure separation (Fig. 3c) or pure shear (Fig. 3d).

In addition to the kinematic conditions of the plastic band, one can assume a plastic response of the material if the strains within this region are perfectly smeared. For concrete, this allows considering a yield surface defined by a Mohr-Coulomb criterion [15] where a tension cut-off is performed due to the enhanced brittleness of concrete in tension. Fig. 4 shows the corresponding yield surfaces for a case under plane stress (Fig. 4a) and plane strain conditions (Fig. 4b, where φ refers to the internal angle of friction of concrete).

It is interesting to note that, in order to respect the normality criterion of increment of strains (associative plasticity), the direction of increment of plastic strains ($\dot{\varepsilon}$) may be different depending on the yield surface and stress state. For plane stress conditions, it is possible to have a strain increment parallel to the compressive direction of loading (Fig. 4a), leading to an apparent reduction of the volume of the plastic band. Such reduction of volume does not however occur in reality, due to the out-of-plane expansion of concrete (Fig. 5a). For concrete under plane strain conditions (Fig. 5b), the out-of-plane expansion is not possible and thus an in-plane expansion occurs (Fig. 5b). In both cases, the resistance (under unconfined conditions) remains identical and equal to the plastic strength of the material (an extended analysis of both cases is presented in Appendix A of this manuscript). Another interesting aspect of this approach is that the size of the plastic band can be

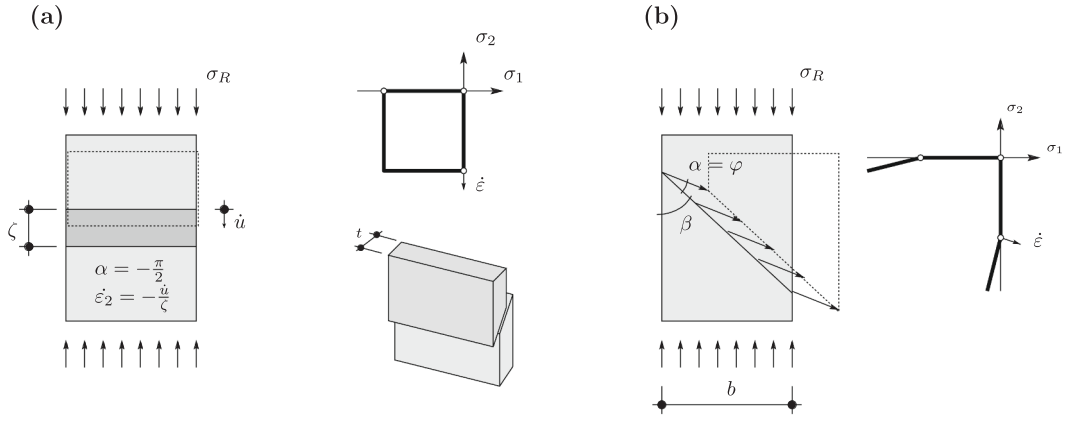

Fig. 5. Concrete prisms under pure uniaxial compression: (a) plane stress conditions; and (b) plane strain conditions.

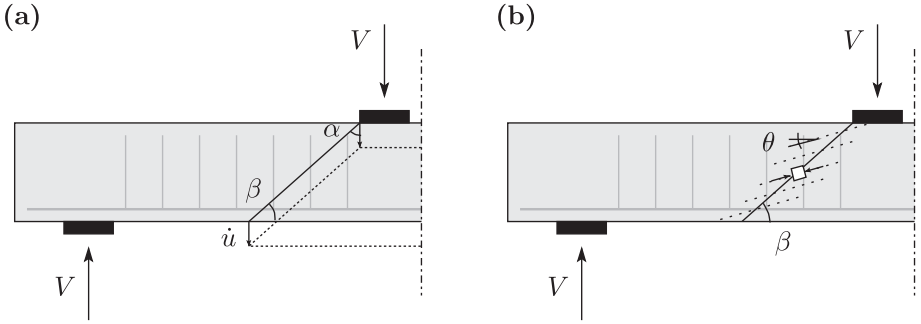

Fig. 6. Analysis of a beam with stirrups according to limit analysis: (a) assumed mechanism; and (b) direction of principal compressive stresses at the yield line.

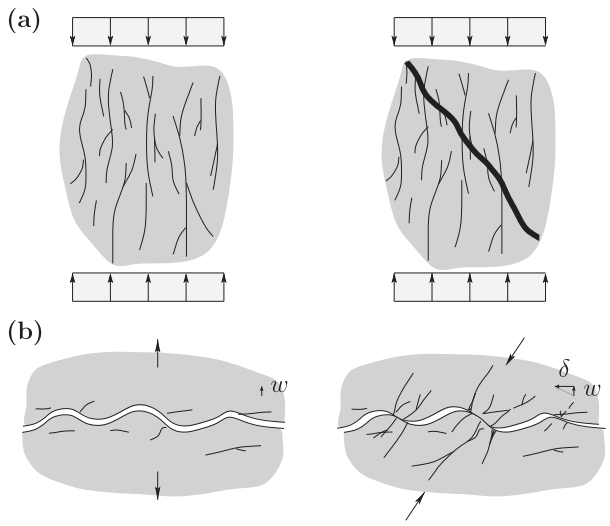

Fig. 7. Development of yield lines and smeared cracking: (a) coalescence of a yield line from previous micro-cracks; and (b) engagement of rough surface contact in an existing crack acting as a yield line.

condensed into a yield line [15], see Fig. 5b. This consideration does not modify the failure load, stress state, orientation of the yield line or kinematics (as thoroughly justified in Appendix A). In this case, the discontinuity is concentrated into a single surface that allows for sliding and separation, as a crack could do.

In addition to the contribution of concrete, the analysis of the resistance by means of limit analysis and yield lines can also involve other materials, as the contribution of reinforcing bars. For instance, in the case of a beam with sufficient stirrups for crack control (refer to Fig. 1b), a kinematics as shown in Fig. 6 (defined by the angle β of the yield line, Fig. 6a) requires plastic dissipation both at the concrete and reinforcement. In such case, the stresses in the concrete develop at a flatter inclination (angle θ in Fig. 6b, where $\theta = \beta/2$ [15]). It is interesting to note that if new cracks are assumed to develop parallel to the principal compressive stress direction (angle θ, see for instance [15,12,17]), a smeared cracking pattern will develop at a different (flatter) angle than the yield line (angle β in Fig. 6b), refer to Fig. 2b.

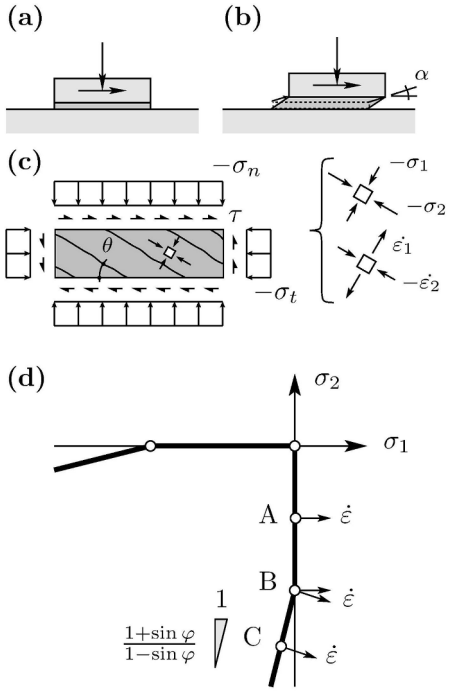

Fig. 8. Analysis of transfer of forces through a plastic band: (a) case investigated; (b) kinematics; (c) (in-plane) stress and strain state; and (d) yield conditions.

3. Development of yield lines and smeared cracking

Following the previous considerations, it can be stated that both yield lines (referring to concentrated cracks) and smeared cracking patterns develop in concrete, and that they can be originated by different conditions:

- Development of a yield line by coalescence of micro-cracks parallel to the principal compressive stresses (Fig. 7a) as for prisms in compression (see Fig. 5 and Appendix A)
- Development of smeared cracking by engagement of crack lips due to sliding of a rough crack surface acting as a yield line (Fig. 2b and Fig. 7b) as for instance in beams with sufficient transverse reinforcement subjected to shear and bending (see Fig. 1b and Fig. 6b)

It is to be noted that the yield line and the direction of principal compressive stresses develop in general at rotated angles (according to the plastic band kinematics). As a consequence, by considering that the smeared cracking pattern develops parallel to the direction of the principal compressive stresses [12], the yield line and the smeared cracking pattern develop also at rotated angles (see Fig. 2b and Fig. 6b). For a perfectly-plastic material, it can be assumed that the resistance is governed only by the strength of the material and that the development of yield lines and smeared cracking patterns has no influence in it. This however does not hold true in general for concrete, where the development of cracking (at the yield line and/or in the smeared cracking region) damages the material and weakens its strength. When the opening of the yield line remains sufficiently low (as in Fig. 7b) the capacity to transfer forces of the yield line is high, allowing for development of smeared cracking and its propagation outside of the yield line region. Such smeared cracking may weaken sufficiently the concrete [9] and be potentially governing for the strength of the member (failure under plane stress conditions outside of the yield line). When the opening of the yield line is on the contrary significant, the capacity to transfer stresses through the yield line becomes governing (Fig. 2a) and sliding can even occur without (or with limited) development of a smeared cracking pattern (Fig. 1a,c).

This distinction is instrumental in the response of structural concrete. When the capacity of the yield line is not governing the strength, the response of the member is controlled by a smeared cracking pattern and the strength is observed not to be (at least noticeably) sensitive to the size of the member [5,18,19]. The unitary strength (strength per unit area) depends thus only on material properties and dimensionless geometric ratios, but does not change with the size of the member. Even if the smeared cracking pattern may potentially weaken the material strength, this effect does not depend on the size of the member as the strains are uniformly distributed [9]:

$$f_R = f_R(\varepsilon_1) \tag{4}$$

It should be noted that this dependence of the strength of the compression field on the state of transversal strain (and associated cracking) holds true in general when sufficient transverse reinforcement is provided so that merging of the cracks and crack localization are prevented.

For larger openings of the crack corresponding to a yield line, the strength may however be limited by the capacity of concrete to transfer forces through a rough surface [4,5]. In this case, for increasing openings of the crack, the engagement of contacts between rough surfaces is

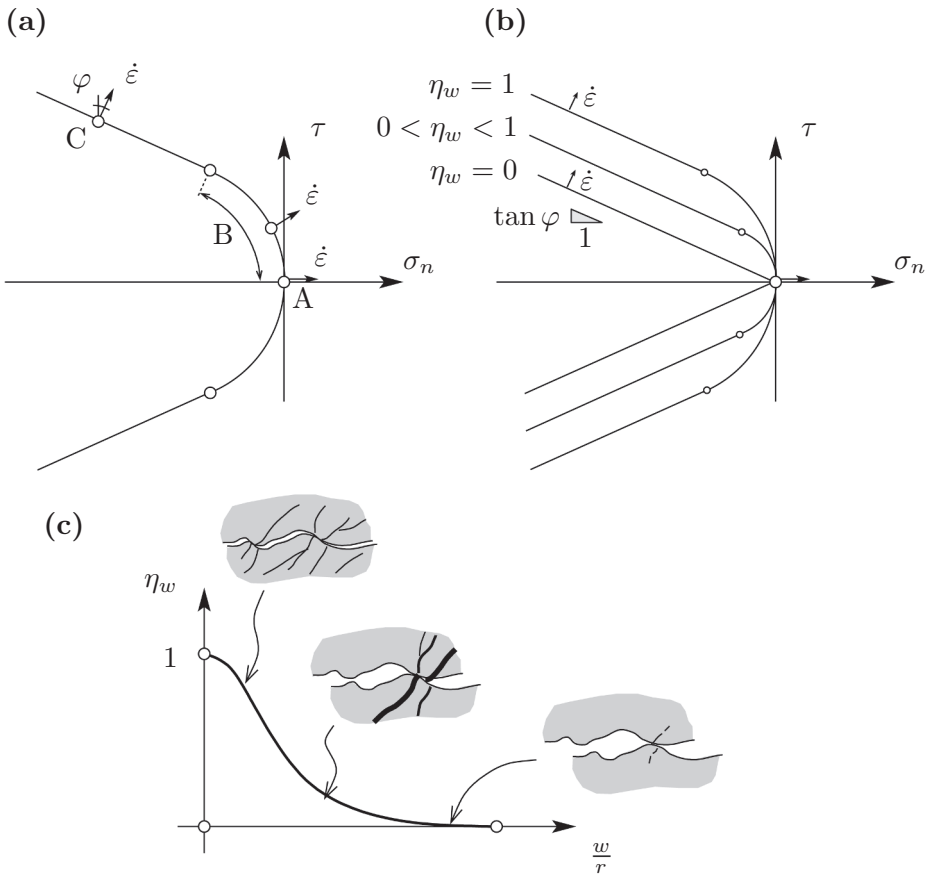

Fig. 9. Capacity to transfer forces according to limit analysis: (a) yield surface; (b) corrected yield surface accounting for opening of yield line; and (c) efficiency factor η_w.

reduced and thus the capacity to transfer forces. As a consequence, when the size of a member increases, the opening of the crack corresponding to a yield line (concentrated discontinuity) also increases proportionally and the unitary strength reduces (provided that the surface roughness (r) is independent of the size of the member [4,5]):

$$f_R = f_R(w/r) = f_R((\varepsilon \cdot s)/r) \tag{5}$$

This dependence has shown to be consistent to describe phenomena where the capacity of a yield line is sensitive to the crack opening, both on the basis of limit analysis [7,20] or according to other approaches [4]. It shall be noted that the roughness of the crack is associated to the properties of the concrete, including aggregate nature and petrography (details can be consulted elsewhere for concrete and mortar mixes [21] or for the influence of aggregate type [22,23]).

4. The transfer of forces in a yield line and the development of smeared cracking

This section presents a comprehensive model based on limit analysis and considering material damage conditions to describe the transfer of forces through a yield line. The approach is eventually validated by comparison to experimental evidence.

4.1. Transfer of forces based on limit analysis

A consistent solution for the transfer of forces through a yield line or plastic band can be developed on the basis of limit analysis for the case shown in Fig. 8a. Provided that a plastic band develops under the combined action of a normal stress (σ_n) and a shear stress (τ), its response is dictated by its kinematics (α, Fig. 8b) and allows determining the internal stress state in the band (Fig. 8c). By taking advantage of the expressions developed for the plastic band and considering plane strain conditions, two cases can be distinguished: a stress state with compression stress only in one direction (cases A and B in Fig. 8d) and a stress state with compression stresses in both in-plane directions (case C in Fig. 8d).

The situation idealized by case A refers typically to a separation condition due to tensile stresses (see also Fig. 4a). More interesting is case B, where the material reaches its yield strength in compression without transversal (in-plane) compression. In this case, assuming a perfectly-plastic behaviour, not all kinematics are possible, but only those respecting the condition $\pi/2 \geq \alpha \geq \varphi$ (to respect the normality criterion to the yield surface [15]). Under these assumptions, the normal and tangential stresses can be expressed as a function of the principal compressive stress (σ_2) as (see Appendix B for full derivation):

$$\begin{aligned} -\sigma_n &= \frac{1}{2} f_{cp}(1 - sin\alpha) \\ \tau &= \frac{1}{2} f_{cp} cos\alpha \end{aligned} \tag{6}$$

In the latter situation (case C in Fig. 8d), concrete develops compressive stresses for both in-plane directions. In this case, under plane strain conditions and associative plasticity, the only possible kinematic response corresponds to $\alpha = \varphi$. Thus, the normal and tangential stresses result (see Appendix B for full derivation):

$$\begin{aligned} -\sigma_n &= \frac{1}{2} f_{cp}(1 - sin\varphi) - \sigma_1(1 + sin\varphi) \\ \tau &= \frac{1}{2} f_{cp} cos\varphi - \sigma_1 \frac{sin\varphi cos\varphi}{1 - sin\varphi} \end{aligned} \tag{7}$$

The solution is plotted in Fig. 9 with reference to the two potential regimes (Appendix B proves it to be an exact solution according to limit analysis). The first regime corresponds to a segment of a circle (point A and region B in Fig. 9a) while the latter corresponds to a straight line (tangent to the circle, refer to point C in Fig. 9a). In both cases, the normality condition of increment of plastic strains to the yield surface is respected (Fig. 9a) and in the second regime the slope defining the increase of tangential strains corresponds to tan(φ). It is also interesting to note that, for the confined regime (point C in Fig. 9a), one part of the tangential stresses depends upon the material strength (first term in Eq. (7)) while the other depends only on the in-plane transversal stress (second term in Eq. (7)). It can thus be demonstrated that shear stresses may develop even if the uniaxial compressive strength were limited or even zero.

Previous works with reference to the transfer of forces during the cracking process in concrete (Carol [24,25], Cendón Franco [26]) have proposed similar shapes defining the failure surface. To that aim, mostly hyperbolic functions are used, providing a smooth transition accounting for the resistance in tension of concrete and a pure-frictional (Coulomb) response. In the proposed formulation, the potential contribution of the residual tensile strength of concrete to the transfer of forces [21] is neglected, although it could also be incorporated (provided that a suitable efficiency factor is defined). It can also be noted that the presented approach is valid until the complete disengagement of the crack lips, when no contacts exist (with the opening of the crack being larger than the meso- and even macro-roughness of the crack [27]).

4.2. Concrete strength and influence of cracking

With respect to the plastic compressive strength to be considered (f_{cp}), this value is normally determined by correcting the material uniaxial strength (f_c, measured in concrete cylinders under rapid-loading conditions) in order to account for its brittleness [12]. Such correction is performed by multiplying the uniaxial compressive strength by a brittleness factor (η_{fc}), accounting for local stress concentrations and stress redistributions (some regions of the concrete are already in their softening phase while the maximum strength is attained in others):

$$f_{cp} = f_c \cdot \eta_{fc} \tag{8}$$

A suitable formulation for this coefficient was proposed by Muttoni [28], accounting for the enhanced brittleness of higher strength concrete and is currently included in *fib*'s Model Code 2010 [29] for the shear design of members with transverse reinforcement or for strut-and-tie and stress field modelling:

$$\eta_{fc} = \left(\frac{f_{c0}}{f_c}\right)^{1/3} \leqslant 1 \tag{9}$$

where f_{c0} is a reference value of the uniaxial compressive strength of concrete ($f_{c0} = 30$ MPa).

In addition to this term, the value of the compressive strength can still require to be reduced by other efficiency factors in order to obtain a suitable estimate of the structural strength of the concrete [30]. This is for instance the case of the influence of distributed cracking on the compressive strength of concrete (η_ε, refer to the compression softening due to the development of distributed transversal cracking in a compression field [9], refer to Eq. (4)), the influence of the casting conditions (η_{is}, due to concrete bleeding and plastic settlement occurring near to the top surface of concrete [30]) or the detrimental influence of ducts or large disturbances (η_D, resulting from local stress concentrations [30]).

In the present case, the capacity of concrete to transfer stresses can potentially be limited by the yield line conditions, depending mainly on the opening and roughness properties of the crack (refer to Eq. (5)). For low openings (Fig. 2b, or when a yield line creates by coalescence of micro-cracking), the engagement of contact between rough surfaces is sufficient to ensure the transfer of forces and to generate a smeared cracking pattern. As the crack further opens (Fig. 9c), this capacity is reduced, associated to more local and higher concentrations of stresses, leading to a less distributed cracking pattern and to an enhanced local damage. For large crack openings (Fig. 9c and Fig. 2a) the capacity is severely reduced or even lost and disengagement of the crack lips may occur (a similar consideration was also proposed by Fisker and Hagsten [7] for the strength of yield lines in cases of shear failures in beams without transverse reinforcement). This phenomenon is suggested to be considered in the following by correcting the uniaxial compressive strength as [20]:

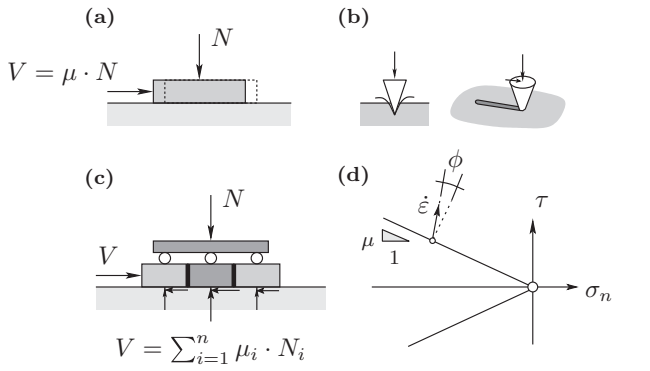

Fig. 10. Pure frictional response in rough contact surfaces: (a) forces; (b) material scratching; (c) response for multiple interfaces; and (e) yield surface and dilatancy.

$$f_{cp} = f_c \cdot \eta_{fc} \cdot \eta_w \tag{10}$$

The influence of the factor η_w on the yield surface is presented in Fig. 9b. A reduced value of the plastic strength (lower values of η_w) shrinks the yield surface, reducing its circular part. For a case with an efficiency factor $\eta_w = 0$ (corresponding to $f_{cp} = 0$), the response in terms of σ_n-τ is governed by friction and is represented by a straight line, passing through the origin of coordinates and where the slope between tangential and normal stresses results:

$$\frac{\Delta\tau}{\Delta(-\sigma_n)} = \frac{sin\varphi cos\varphi}{1 - sin^2\varphi} = tan\varphi \tag{11}$$

Such relationship can be considered as a lower-bound of the actual strength, occurring without development of smeared cracking. It can be noted that for the typical value assumed for the internal angle of friction of concrete ($\varphi = 37.2°$ [15]), it results a slope tan(φ) = 0.76. This value is in fair agreement to the experimental values reported by Yoo et al. [31] on shear friction on concrete surfaces, varying between 0.71 and 0.77 (for a concrete of $f_c = 61.1$ MPa and with varying levels of normal stress between $\sigma_n = 0.76$ MPa and $\sigma_n = 2.3$ MPa).

4.3. Frictional response of concrete

The response of concrete in case of $\eta_w = 0$ has some analogies with the phenomenon of friction in rough surfaces, although significant differences persist. In case of a pure frictional response, Fig. 10a, the force required to generate a slip between two surfaces can be assumed to be equal to a friction coefficient times the normal force between them (the

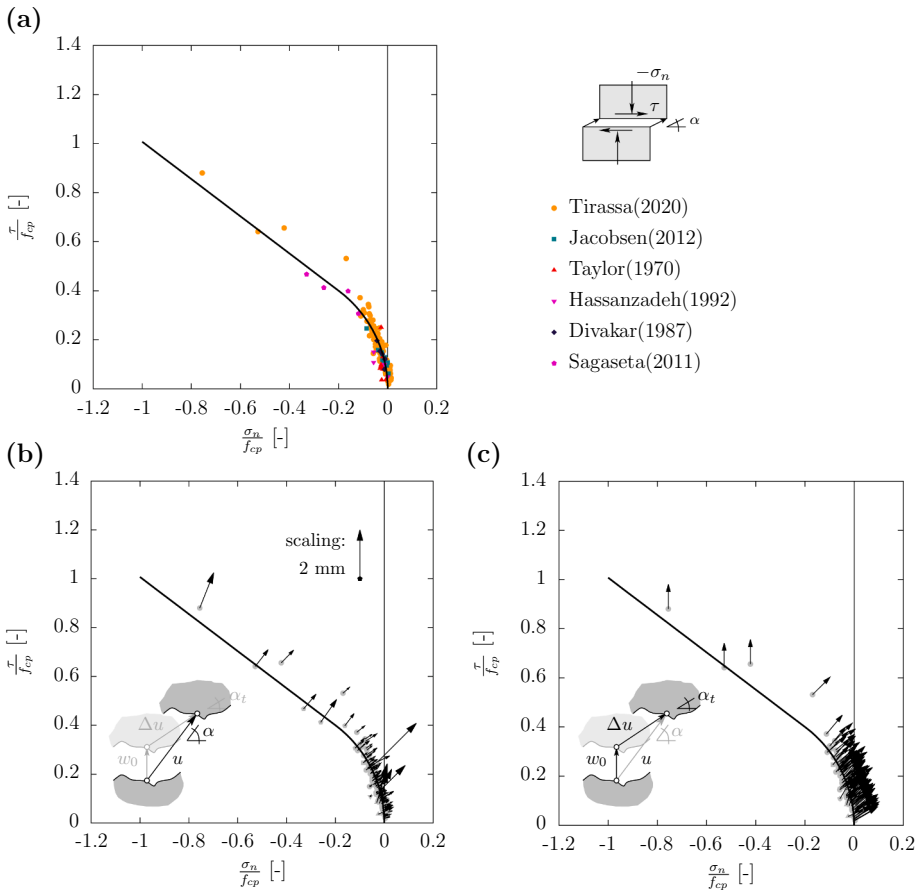

Fig. 11. Yield surface and comparison to test results: (a) comparison to test with initial crack opening (w_0) followed by Mixed Mode kinematics; (b) direction of total displacement (α, shown as vectors proportional to total displacement); and (c) increment of displacement in the direction of the Mixed Mode kinematics (α_t).

value of the friction coefficient μ being variable depending also on the static or dynamic response). In the case of a pure frictional response, there is however a significant difference with respect to the plastic response, as there is no need for a minimum dilatancy (refer to the condition $\alpha \geq \varphi$ in the increment of plastic deformations for plane strain conditions). This is justified by the fact that one part of the material can scratch the other, and the scratched material is deposited at the sides, see Fig. 10b.

In fact, the relative displacement can develop for values $\alpha \geq 0$, but this parameter is not controlled during the characterization of the roughness properties. It can thus be noted that for cases where $\alpha = \varphi$, a pure frictional response could be identical to the perfectly-plastic one. However, for other (lower) values of α, the normality condition to the yield surface is lost and consequently the unicity in the response [15]. The loss of unicity is a well-known issue for instance in masonry works, where the frictional strength depends upon the state of initial stresses (see for instance Fig. 10c, where the frictional resistance depends upon the distribution of normal forces in the different contact surfaces [32]).

In an analogous manner to the plastic response, the pure frictional capacity can also be described in terms of a yield surface (Fig. 10d), where the strain increments are thus not necessarily normal to the surface but develop at a certain angle ($\varphi \geq \phi \geq 0$). For concrete, models accounting for a pure frictional response consider however the degradation of the friction coefficient (μ) up to residual values for increasing material damage due to cracking [25].

4.4. Validation of failure surface against test results

The proposed approach is compared in Fig. 11a to the test results collected by Tirassa [33] on specimens aimed at the transfer of forces through cracked concrete surfaces (including the experimental series of [22,33–37]). As shown in Fig. 11a, only tests with a kinematics corresponding to an initial crack opening (w_0, Mode I) followed by a linear Mixed-Mode kinematics are considered (constant angle α_t after initial crack opening). The database considers both tests where sliding at the primary crack led to failure or where secondary cracking developed (outside of the notch regions) and governed the response. The comparison (Fig. 11a) shows fine agreement for the two regimes of behaviour (unconfined and confined response).

For the comparison presented, the efficiency factor related to the crack opening (Fig. 9c) in Eq. (10) is evaluated by means of the following expression, considering a hyperbolic decay with respect to the crack opening:

$$\eta_w = \frac{1}{1 + 100 \cdot \frac{w}{r}} \tag{12}$$

where the crack opening (w) considered corresponds to the experimentally-measured one at maximum shear force and the parameter r refers to the equivalent surface roughness, evaluated by means of the expression proposed by Cavagnis et al. [14] (additional consideration on surface roughness can be consulted elsewhere [21,38]):

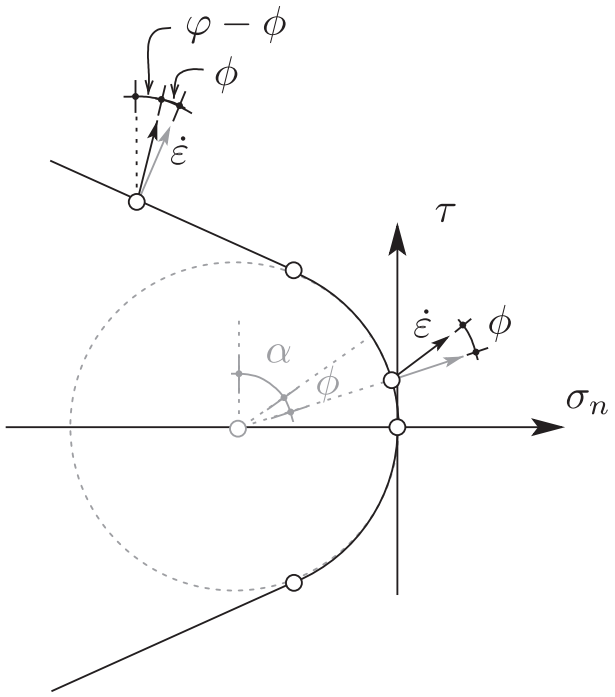

Fig. 12. Consideration of dilatancy: yield surface and strain increment.

$$r = d_{g0} + d_g \cdot min\left((60/f_c)^2, 1\right) \tag{13}$$

It can be noted that the proposed expression for coefficient η_w (Eq. (12)) has similarities with the one proposed by Brantschen et al. [39], that was mechanically derived for a similar case (mechanical engagement of contact between ribs and cracked concrete).

4.5. Consideration of actual crack kinematics and comparison to selected test data

In addition to the failure criterion, Fig. 11b depicts for each test a vector indicating the opening and sliding components at maximum shear strength (vector length proportional to the total displacement, where the increment of crack opening is plotted in the σ_n-axis and the increment of sliding in the τ-axis). The results show that the vector of total displacements is reasonably well approximated by a normal to the yield surface. Nevertheless, deviations are found, with most values below a scatter of 15°. These deviations can be explained to a large extent by the fact that the loading path is not proportional (see sketch of displacements in Fig. 11b) but depends upon the initial crack opening (w_0 and α_t, see sketch of displacements in Fig. 11c). This fact can be clearly seen in the diagram of Fig. 11c, where the tangent increment of displacements is plotted for the different tests (angle α_t instead of angle α). As it can be noted, the displacement increment is not perpendicular to the yield surface, particularly when high stresses are developed (corresponding to values $\alpha_t \approx 0$, related to pure shearing displacement after the initial crack opening). Due to this reason, the response of a member depends on the displacement path followed [27], and the unicity on the response is lost.

On the basis of these considerations, the influence of the initial crack opening on the response can be accounted for in a simplified manner by considering a dilatancy angle (see Fig. 12). This consideration makes the strain increment not to be perpendicular to the yield surface but to develop at a certain angle (ϕ, see Fig. 12).

Under such assumption, the stress state and transferred forces can be directly determined for a given kinematics including its initial crack opening. For instance, in the case of unconfined response (case B in Fig. 9), the stress–strain relationships result (see Fig. 12):

$$\begin{aligned} -\sigma_n &= \frac{1}{2} f_{cp}(1 - sin(\alpha + \phi)) \\ \tau &= \frac{1}{2} f_{cp} cos(\alpha + \phi) \end{aligned} \tag{14}$$

With $\tan(\alpha) = w/\delta$ (valid for $\pi/2 \geq (\alpha + \phi) \geq \varphi$), while for confined cases ($\alpha = \varphi - \phi$, case C in Fig. 9), the response depends upon the confinement pressure.

In addition to the characterization of the stress state at failure by means of the yield surface, if the elastic activation of the interlock forces is neglected (see a detailed discussion in [21,27]), the strength provided by the yield surface can be used to describe the complete aggregate interlock transfer. This approach is compared in Fig. 13 to three experimental series tested by Jacobsen et al. [34] with different initial crack openings and kinematics. This is done by using Eq. (13) (neglecting non-contact situations and considering a variable value of the angle α according to the actual kinematics) and by approximating the dilatancy angle on the basis of the following expression (with the condition that $\phi \leq \varphi$):

$$\phi \approx 10° \cdot \left(1.1 + 20\sqrt{\frac{w_0}{r}}\right) \tag{15}$$

The tests of Jacobsen can be seen as a good validation of the model for relatively low crack openings and with reference to an unconfined response. With respect to the other potentially governing regime (confined response, point C in Fig. 8c), the tests by Calvi et al. [40] are presented in Fig. 14. These tests refer to concrete panels cracked in pure tension and where the shear stress was increased thereafter (shear stresses only transferred by aggregate interlocking as reinforcement bars were placed inside of plastic tubes). Two nominally identical tests are presented in Fig. 14, whose sole difference was the concrete uniaxial strength ($f_c = 38$ MPa for specimen PC4, Fig. 14a, and $f_c = 104$ MPa for specimen PC16, Fig. 14b).

In both cases, very large crack openings and sliding occurred at the yield line (primary tension crack, up to almost 3 mm of opening and 13 mm of crack sliding) which led to very low values of the angle α (at failure, $\alpha = 11°$ for PC4 and $\alpha = 14°$ for PC4). Such values, significantly below the internal angle of friction, are reasonable accounting for the

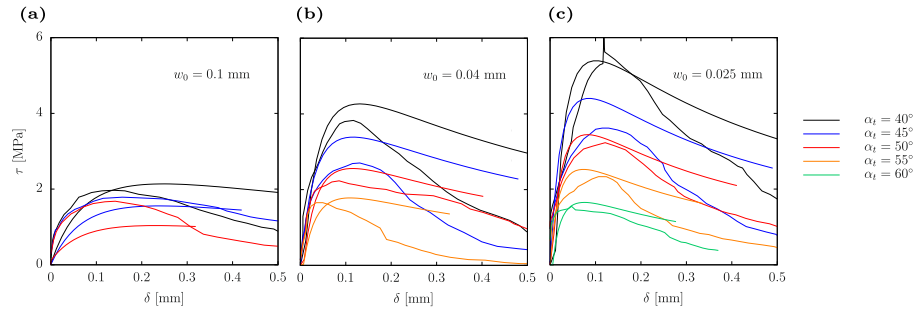

Fig. 13. Comparison of transfer stresses with the tests of Jacobsen [34] for different crack openings: (a) $w_0 = 0.1$ mm; (b) $w_0 = 0.04$ mm; and (c) $w_0 = 0.025$ mm.

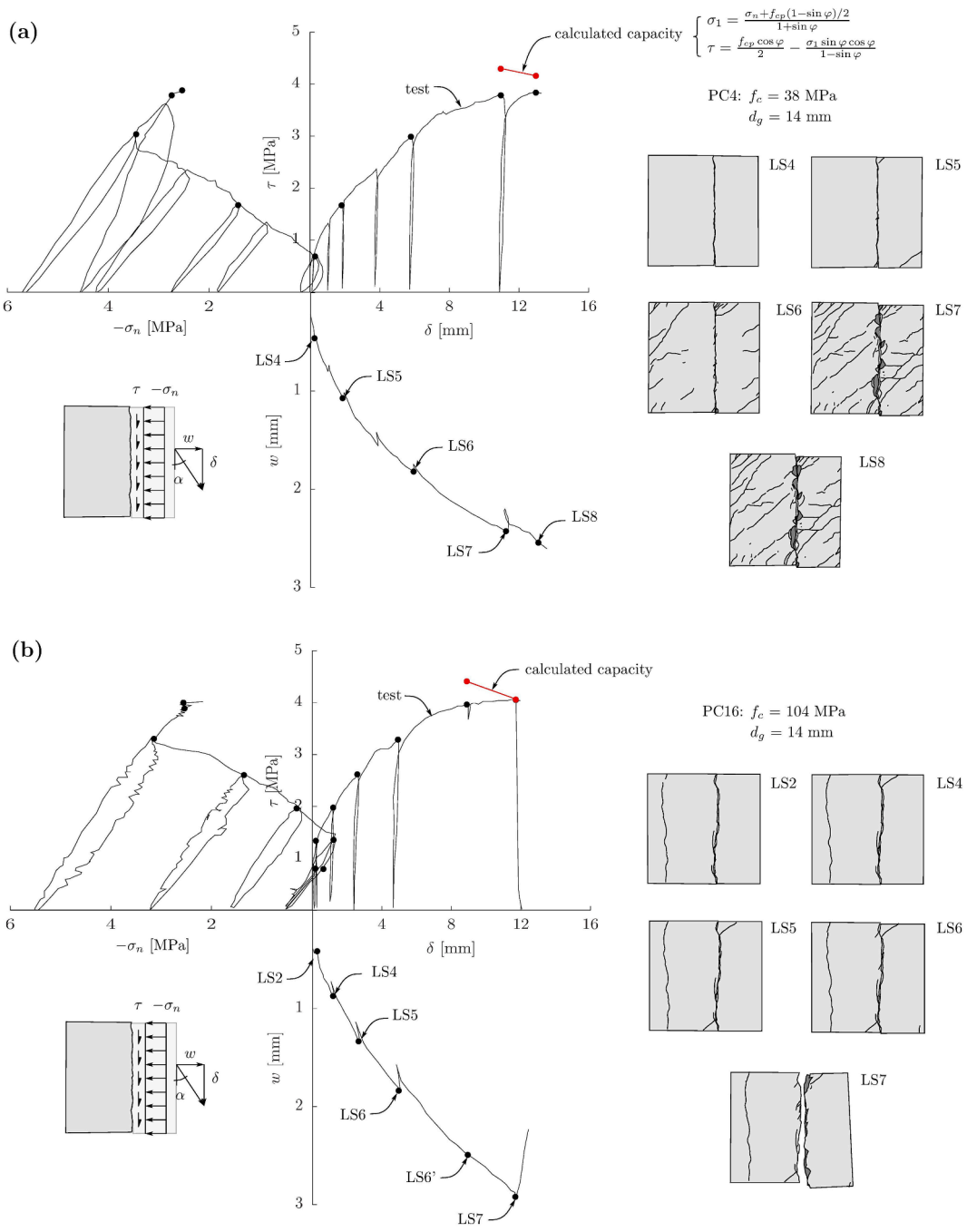

Fig. 14. Comparison of proposed approach with tests by Calvi et al. [40] (measured crack opening, slip and acting shear and normal stress at the crack as well as crack patterns at selected load steps): (a) test PC4 and comparison to calculated capacity (Eq. (7)); and (b) test PC16 and comparison to calculated capacity (Eq. (7)).

value of the dilatancy angle developed under such conditions ($\phi = \varphi$, refer to Eq. (15)). As a consequence, the concrete at the yield line can be assumed to be severely damaged (refer to coefficient η_w), although its contribution is not zero and a significant fraction of the force is transferred by friction associated to the in-plane confinement pressure (regime defined by a straight line in Fig. 12). As it can be observed in Fig. 14, a plastic plateau was reached for both specimens in the shear stress-to-slip diagram. When the strength of this plateau is compared to the response of the confined regime (refer to the red lines in Fig. 14 calculated by means of Eq. (7)), one can note a very accurate prediction of the resistance, with all parameters calculated consistently with the previous assumptions (refer to the analyses presented in Fig. 11 and Fig. 13).

It is also interesting to note in Fig. 14 the crack patterns developed by both specimens. For specimen PC4 (Fig. 14a), with moderate concrete strength, the contact stresses at the yield line led to the development of an inclined micro-cracking pattern in the vicinity of the yield line already for low loading stages (refer for instance to the cracking pattern for LS6 in Fig. 14a, in agreement to the pattern described in Fig. 2b). Failure occurred eventually without physical disengagement of the crack lips and by crushing of the concrete near to the yield line (refer to crack patterns and crushed regions for LS7 and LS8 in Fig. 14a). Outside of the yield line, an inclined smeared cracking pattern also developed, governed by the reinforcement provided in this region (significantly higher than at the yield line [40]). On the contrary, for specimen PC16 (Fig. 14b) with a relatively high concrete strength ($f_c = 106$ MPa),

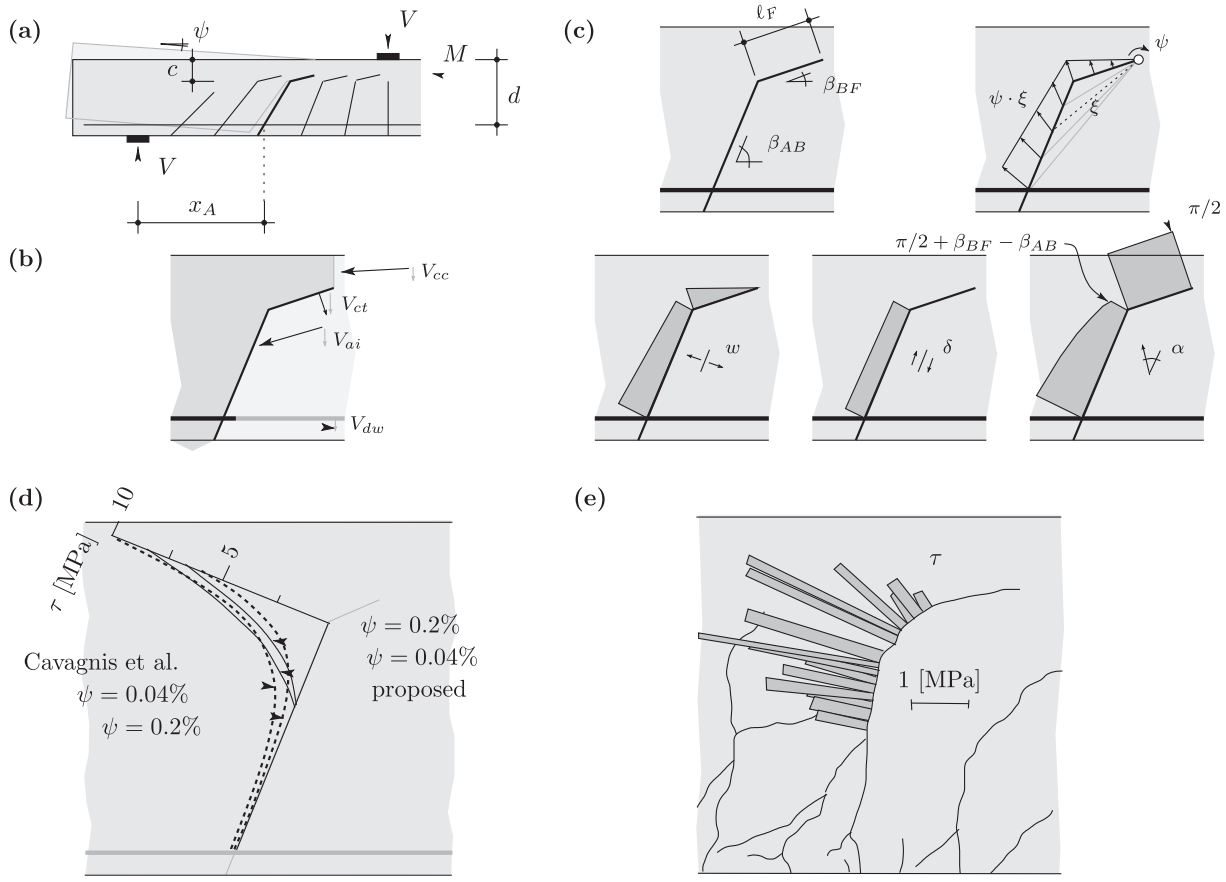

Fig. 15. Contribution of aggregate interlock to the shear strength of beams: (a) physical model of the Critical Shear Crack Theory; (b) shear carrying actions (V_{cc}: compression chord, V_{ct}: residual tensile strength, V_{ai}: aggregate interlock, V_{dw}: dowel action); (c) critical shear crack kinematics, including opening (w), sliding (δ) and opening angle (α); (d) calculated tangential stresses due to aggregate interlocking (according to Cavagnis et al. [14] and to the proposed approach for $f_c = 40$ MPa, $d = 550$ mm, $d_g = 16$ mm, $\rho = 1\%$ and $x_A = 4d$); and (e) calculated values of tangential stresses by Cavagnis et al. [13] (specimen SC70) from measured crack kinematics and Walraven's model [46]for aggregate interlock.

failure occurred by disengagement of the crack lips (refer to Fig. 2a and to the crack pattern for LS7 in Fig. 14b).

As it can be noted from these comparisons, both cases with relatively low and large crack openings (as Jacobsen et al. [34] and Calvi et al. [40] respectively), governed by different regimes of behaviour (unconfined or confined conditions) and with different failure modes (smeared cracking conditions or crack localization) can be consistently explained on the basis of the same set of assumptions.

5. Implications for elements without transverse reinforcement

One of the most important applications of interlock models refers to the contribution of cracked concrete to transfer shear forces in beams and slabs without transverse reinforcement [41]. An extensive review of this phenomenon (as well as the contribution of other potential shear-transfer actions as dowelling action [42], residual tensile strength of concrete [43] or the inclination of compression chord [44]) can be consulted elsewhere [45]. In the following, the role of aggregate interlocking in the shear resistance will be investigated within the frame of the Critical Shear Crack Theory (CSCT) [4,5] by using the model introduced in the previous sections.

According to the CSCT, the shear resistance of a concrete member without transverse reinforcement is governed by the development of a critical shear crack localizing the strains [4]. Such critical shear crack, representing a discontinuity with the capacity to open and to slide, can in fact be considered as a yield line, potentially sensitive to the disengagement of the crack lips. For calculation of the aggregate interlock forces developing at the critical shear crack, its shape and kinematics are governing [13,14,49,38] together with the size of the aggregates and crack roughness [47,48]. In the following, the characterization of the geometrical parameters defining the shape and kinematics of the critical shear crack derived by Cavagnis et al. [13,14] on the basis of test observations will be considered. The critical shear crack is thus considered to have a bilinear crack shape, whose kinematics is characterized by the location of the centre of rotations at the tip of the critical shear crack (Fig. 15a-c). On the basis of these assumptions, the opening and sliding of the critical shear crack can be directly determined as shown in Fig. 15c, allowing to calculate the contribution of the various potential shear-transfer actions (see Fig. 15b, a detailed approach for their calculation can be consulted elsewhere [13,14]).

As it can be noted, the crack opens along its complete length, but only slides along its quasi-vertical branch, engaging aggregate interlocking in this region [5]. A detailed analysis of the contribution of aggregate interlock in terms of shear stress at the crack, is shown in Fig. 15d for a given case ($f_c = 40$ MPa, $d = 550$ mm, $d_g = 16$ mm, $\rho = 1\%$ and $x_A = 4d$, see [14]), presenting two levels of deformation in the

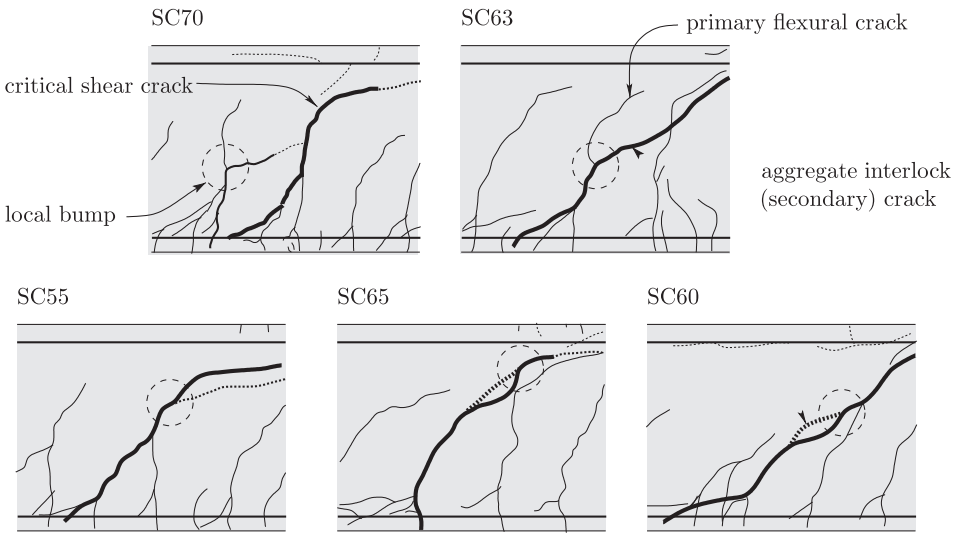

Fig. 16. Development of secondary cracks due to high aggregate interlocking stresses originated by local bumps in the shape of the primary flexural crack.

reinforcement ($\psi = 0.4‰$ and $\psi = 2‰$). According to the laws provided by Cavagnis et al. [14] (approximating the general model of Walraven [46]), the shear stresses originated by aggregate interlock are relatively high near to the point of change of slope in the critical shear crack and decay thereafter due to the increasing opening of the cracks (refer to the dashed lines in Fig. 15d). The approach to calculate the contact stresses in a yield line presented in this paper is also compared in the same figure (refer to the solid lines in Fig. 15d). For that purpose, the angle of relative slip (α) is calculated (Fig. 15c) allowing to determine the interlock stresses together with the opening of the crack (an average value of the dilatancy angle $\phi = 17°$ is assumed for simplicity reasons, refer to Fig. 11b). It is interesting to note that the minimum value of α is in all cases higher than the internal friction angle of concrete ($\varphi = 37.2°$), leading the unconfined response of concrete to be governing. Comparing both analyses, it can be observed that the maximum value of the interlock tangential stresses is relatively similar. However, the approach of Cavagnis et al. [14] leads to a steeper decay of the stresses following an asymptotic transition to zero, while in the approach based on limit analysis considerations, the stresses do not decrease so rapidly but can reach values equal to zero. The resultant of both aggregate interlock stress distributions is similar in terms of total (integral) contribution, but the consideration of a higher concentration of stresses in the top part of the quasi-vertical branch of the crack (corresponding to the approach based on limit analysis), seems to be more consistent with the calculated stresses from the actual crack kinematics (see Fig. 15e according to [13]).

It is also interesting to note with respect to the assumed kinematics (refer to angle α in Fig. 15c), that all points have higher values than the internal angle of friction of the concrete. This results in possible solutions according to the approach based on limit analysis, even if no dilatancy (ϕ) due to a previous crack opening were considered (which could be the case at the point of change of slope in the crack, corresponding to the lowest angle α and $w_0 = 0$). In case lower values of the angle α result ($\alpha < \varphi$-ϕ), no solution would be possible. Actually, such cases can occur in practice and correspond to crack patterns as those shown in Fig. 16 for selected critical shear cracks of the test programme of Cavagnis et al. [14]. In these cases, the *meso*-roughness of the crack leads to undulations of its shape, generating local bumps. When such bumps lead to low values of the angle α (depending on the crack shape and kinematics), high interlock forces are generated, leading to the development of a secondary crack at the edge of the bump, see Fig. 16. Such cracks, associated to the local interlock forces, can in many cases lead to an unstable propagation and to the eventual failure of the specimen (an extended discussion on the basis of the potential crack development types can be consulted elsewhere [1,3]). When sufficient transverse reinforcement for crack control is however provided, the cracks may progress in a stable manner and develop as part of the secondary (inclined) cracking pattern (Fig. 1b).

6. Conclusions

This manuscript investigates on the capacity of cracked concrete to transfer stresses. Its main conclusions are summarized below:

(1) A crack in a concrete member, representing a discontinuity with the capacity to open and to slide, can be considered as a yield line and is potentially sensitive to the disengagement of its crack lips. Such yield line may form by coalescence of existing micro-cracks or from external actions (typically previous tensile stresses). In the latter case, when an existing rough crack suffers a sliding movement, it may engage contact forces due to aggregate interlocking and generate a set of secondary smeared cracks at a rotated angle (according to the principal stress direction).
(2) The capacity of a yield line to transfer forces by aggregate interlocking is observed to be dependent on the crack opening and surface roughness. For large crack openings and/or steep kinematics (high crack openings compared to crack slip), a disengagement of the crack lips may occur, disabling the capacity to transfer forces through a yield line and governing thus the strength.
(3) When smeared cracking conditions govern the strength (micro-cracking leading to the coalescence of a yield line or secondary cracks generated by aggregate interlock), the strains are smeared and the strength is theoretically not dependent on the size of the member (in agreement to classical assumptions of limit analysis). In these cases, the capacity of concrete to transfer stresses may be softened depending on the transverse strains and the strength is

governed by conditions outside of the yield line (progression of smeared cracking).

(4) When disengagement of crack lips governs the strength, the capacity to transfer stresses depends upon the crack opening of the yield line. This implies a size effect for members subjected to the same level of deformation, as crack spacing and thus crack openings increase with the size of the member. A similar effect also occurs for increasing member strains, associated to larger crack openings of the yield line.

(5) A consistent approach to this phenomenon can be formulated by considering the influence of the opening of a concentrated crack (with respect to its roughness) in the resistance of a yield line according to limit analysis. This allows considering the different failure modes (smeared cracking due to engagement of contact forces in a rough surface or loss of rough surface engagement) and governing regimes (concrete under confined or unconfined conditions).

(6) A consistent formulation following this approach is presented in this work, including the concepts of material damage, crack dilatancy and kinematical path. Such approach is shown to lead to sound results for cases with high and low crack openings and associated to different failure modes.

(7) The concepts of transfer of forces through a yield line and the conditions to develop secondary cracking by engagement of interlock forces are shown to allow interpreting the response of members in shear and to be in agreement to experimental measurements. Also, the kinematical angles developed in a shear crack allow explaining the formation of secondary cracks related to aggregate interlock and potentially governing the structural strength of members without transverse reinforcement.

CRediT authorship contribution statement

Miguel Fernández Ruiz: Conceptualization, Methodology, Software, Validation, Formal analysis, Investigation, Resources, Writing - original draft, Writing - review & editing, Visualization, Project administration, Funding acquisition.

Declaration of Competing Interest

The authors declare that they have no known competing financial interests or personal relationships that could have appeared to influence the work reported in this paper.

Acknowledgements

This work has been performed with the financial support of the Swiss National Science Foundation, research grant #200021_169649.

The author would like to thank Prof. Linh Cao Hoang (DTU, Denmark) and Dr Duarte Miguel Viula Faria (consulting engineer, Switzerland) for the discussions and review of the limit analysis approach. Also, special thanks are given to Prof. Aurelio Muttoni (Ecole Polytechnique Fédérale de Lausanne) for the detailed reading of the manuscript and his valuable comments and suggestions. Finally, the author would like to acknowledge Dr Max Tirassa (former PhD candidate at Ecole Polytechnique Fédérale de Lausanne, Switzerland) for the collection of tests used in Fig. 11.

Appendix A. Concrete prisms in pure compression

In this Appendix, the strength of a concrete prism subjected to a uniaxial state of stress is investigated with reference to plane strain and plane stress conditions. Upper-bound solutions are obtained by means of two approaches for the analysis of a mechanism: energy rate balance (work rate equation) and equilibrium conditions of a free-body. The latter approach is an unusual manner to obtain upper-bound solutions, but it is shown to be faster to calculate failure loads in many cases and also to investigate on the stress state at failure. The solutions are eventually compared to a lower-bound solution, allowing to discuss on the exact solution according to limit analysis. For the analyses presented, compressive stresses are considered to be negative.

A.1. Upper-bound solution of a plane-strain case by energy rate balance

Failure of a concrete prism under plane strain conditions is investigated in Fig. 17a-b by means of a potential failure mechanism. The mechanism comprises a plastic band with a height ζ developing at an angle β with respect to the direction of loading. This mechanism leads to the displacement field increment shown in Fig. 17b (characterized by the angle α). Under these assumptions, the power (energy rate) introduced in the system results:

$$P_e = -\sigma \cdot b \cdot t \cdot \dot{u} \cdot cos(\alpha + \beta) \tag{16}$$

While the rate of dissipated energy results (assuming that failure occurs under unconfined conditions, point B in Fig. 8):

$$P_i = \int \tilde{\sigma} \cdot \tilde{\dot{\varepsilon}} dV = f_{cp} \cdot \frac{1}{2} \frac{\dot{u}}{\zeta} (1 - sin\alpha) \cdot \frac{b}{sin\beta} \cdot \zeta \cdot t = \frac{1}{2} f_{cp} \cdot \frac{1 - sin\alpha}{sin\beta} b \cdot t \cdot \dot{u} \tag{17}$$

where f_{cp} refers to the equivalent plastic strength of concrete. It is interesting to note that none of the previous equations depends on the size of the plastic band, and the same conditions could result by considering a concentrated yield line as the one shown in Fig. 17c.

On the basis of these expressions, and by means of the work rate condition, failure can be ensured to happen for a kinematically admissible mechanism when:

$$P_e \geqslant P_i \tag{18}$$

which results into:

$$-\sigma \geqslant \frac{1}{2} f_{cp} \cdot \frac{1 - sin\alpha}{sin\beta \cdot cos(\alpha + \beta)} \tag{19}$$

The best solution for the failure stress is thus obtained by minimizing the previous equation (minimum value of an upper-bound solution). This can be done in a general manner, although requiring numerical means or a quite complex analytical treatment. Alternatively, assuming that failure occurs at maximum dissipation conditions ($\alpha = \varphi$ in Fig. 17d, governing condition [15]), the solution can be obtained by maximizing the term $\sin(\beta) \cdot \cos(\varphi +$

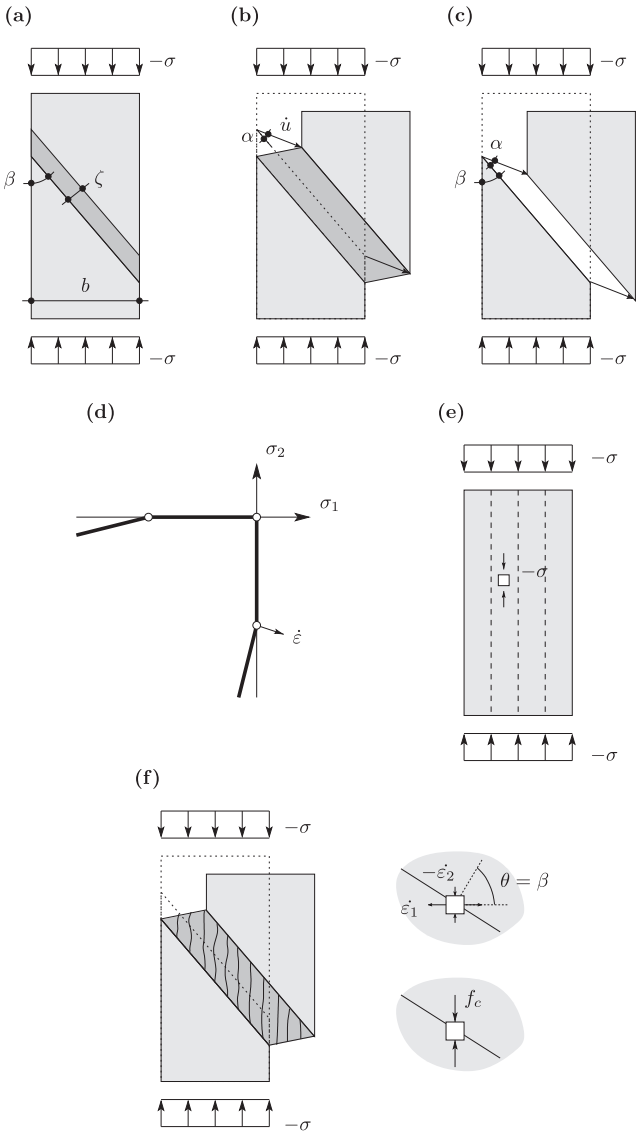

Fig. 17. Response of a concrete prism in pure compression: (a) geometry and definition of failure band; (b) kinematics at failure; (c) case of a concentrated yield line; (d) plasticity surface and normality criterion; (e) resulting stress field; and (f) associated cracking pattern and corresponding stress state.

β) which results in $\tan(\varphi) = \cot(2\beta)$ and thus:

$$\beta = \frac{\pi}{4} - \frac{\varphi}{2} \tag{20}$$

By introducing this value in the previous equation, failure is ensured if:

$$-\sigma \geqslant f_{cp} \tag{21}$$

A.2. Lower-bound and exact solutions of a plane-strain case

Other than the upper-bound solution, a lower bound can be determined on the basis of the simple stress field shown in Fig. 17e. In this case, a lower-bound of the strength can be ensured provided that the following condition is respected (fulfilment of equilibrium and yield condition of the material at every location):

$$-\sigma \leqslant f_{cp} \tag{22}$$

By comparing the upper- and lower-bound approach, one can note that the exact solution can be determined as the intersection between the upper- (Eq. (21)) and lower-bound solutions (Eq. (22)):

$$-\sigma = f_{cp} \tag{23}$$

Corresponding to a licit stress field (lower-bound solution) which is compatible to a kinematically admissible mechanism (upper-bound solution). Such strength (Eq. (23)) corresponds thus to the exact solution according to the theory of plasticity, which can be considered to be unique due to the

normality conditions to the yield surface.

A.3. Upper-bound solution of a plane-strain case by equilibrium of a free-body

An alternative approach for calculating the failure load consists on imposing directly the equilibrium conditions in the plastic region (Fig. 17f). This approach is in fact much simpler than the one presented in section A.1 (based on the work rate equation), as it yields directly that σ_2 has to develop parallel to the loading direction and thus:

$$\theta = \beta = \frac{\pi}{4} - \frac{\varphi}{2} \tag{24}$$

This leads thus to $-\sigma \geq f_{cp}$ without the need of performing any minimization process and leading directly to the exact solution according to limit analysis (the stress state within the plastic band and at its boundaries is in agreement to the lower-bound solution of Fig. 17e).

Other than the easiness of such an equilibrium approach, it further allows for obtaining directly the stress field and strain increment field, see Fig. 17f. It can be noted that the stresses in the plastic region results parallel to the loading direction (as imposed) and that the concrete dilates with a transversal expansion rate equal to approximately four times ($\approx (1 + \sin(\varphi))/(1 - \sin(\varphi))$) the longitudinal shortening rate.

A.4. Exact solution of a plane-stress case

With respect to a plane stress situation, an upper-bound solution can also be easily obtained for the mechanism shown in Fig. 5a on the basis of the equilibrium of a free-body or by balance of energy rates. The former solution is again obtained in a simpler manner, by imposing that the stress direction remains parallel to the external load ($\alpha = \pi/2$), thus resulting directly into $-\sigma \geq f_{cp}$ as an upper-bound of the strength.

With respect to the other approach (balance of energy rates), the rate of external energy results:

$$P_e = -\sigma \cdot b \cdot t \cdot \dot{u} \tag{25}$$

While the rate of internal dissipated energy results:

$$P_i = \int \tilde{\sigma} \cdot \tilde{\varepsilon} dV = f_{cp} \cdot b \cdot t \cdot \zeta \cdot \frac{\dot{u}}{\zeta} \tag{26}$$

On the basis of the work rate equation ($P_e \geq P_i$), it results that $-\sigma \geq f_{cp}$ is an upper-bound solution of the strength, thus giving rise to the same exact solution as for the plane strain case ($-\sigma = f_{cp}$, same lower-bound solution of Fig. 17e applicable).

Appendix B. Interface stresses in a failure band

In this Appendix, the interface stresses developing in a failure band are derived on the basis of limit analysis by developing an exact solution. The stress state is calculated according to the kinematics shown in Fig. 8a and considering two limit cases: an unconfined response of concrete (point B in Fig. 8d) and a confined response (point C in Fig. 8d). As for Appendix A, compressive stresses are considered to have a negative sign.

B.1. Unconfined response

The stress state corresponding to an unconfined response is shown in Fig. 18a. For the considered kinematics (Fig. 8b), the principal compressive stresses develop parallel to the angle θ (Fig. 3b), corresponding to the direction of $\dot{\varepsilon}_2$ (increment of principal compressive strain). In the other direction ($\dot{\varepsilon}_1$) the in-plane stress is equal to zero (refer to point B in Fig. 8d).

On the basis of this stress field, the stresses at the interface of the failure band (refer to σ_n and τ in Fig. 8c) can be calculated by equilibrium considerations as:

$$\begin{aligned} \sigma_n &= \sigma_2 sin^2\theta \\ \tau &= \sigma_2 sin\theta cos\theta \end{aligned} \tag{27}$$

It can be noted that such stresses can be expressed in a more convenient manner in terms of the angle α (where $\theta = \pi/4 - \alpha/2$), resulting into:

$$\begin{aligned} \sigma_n &= \frac{1}{2}\sigma_2(1 - sin\alpha) \\ \tau &= \frac{1}{2}\sigma_2 cos\alpha \end{aligned} \tag{28}$$

which, considering the stress state at the plastic surface ($-\sigma_2 = f_{cp}$, refer to point B in Fig. 8d), it results (indistinct sign of shear stress):

$$\begin{aligned} -\sigma_n &= \frac{1}{2}f_{cp}(1 - sin\alpha) \\ \tau &= \frac{1}{2}f_{cp} cos\alpha \end{aligned} \tag{29}$$

B.2. Confined response

The same approach can be followed for the confined regime (point C in Fig. 8d), by considering:

$$-\sigma_2 = f_{cp} - \sigma_1 \frac{1 + sin\varphi}{1 - sin\varphi} \tag{30}$$

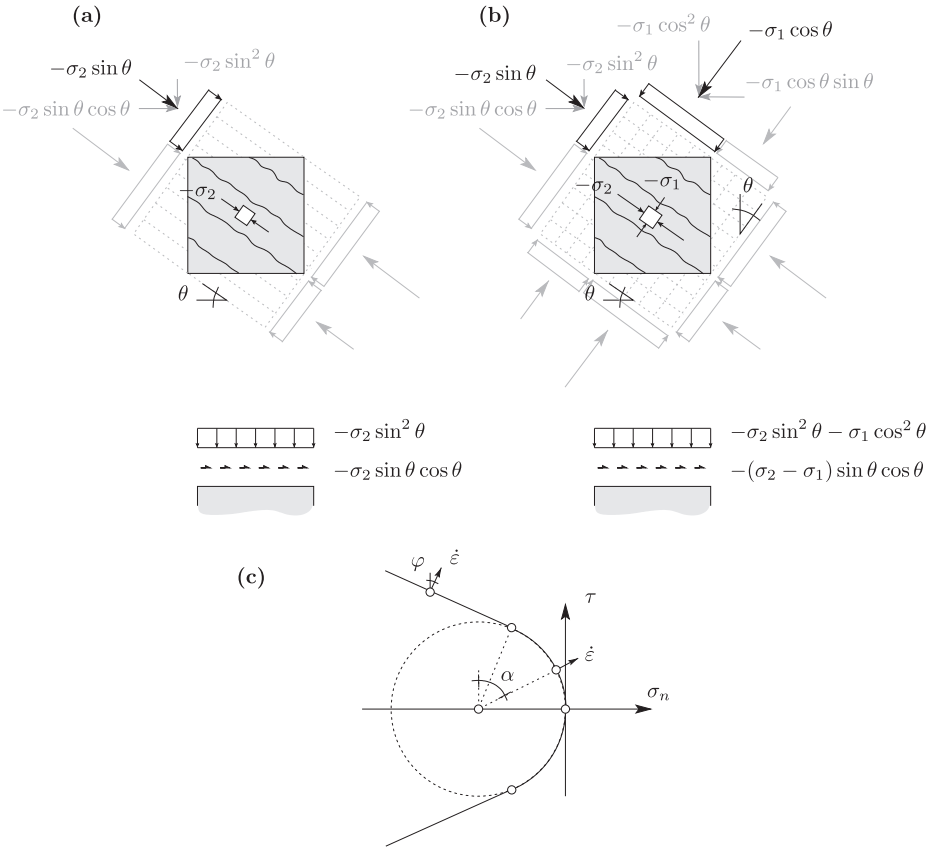

Fig. 18. Stress field in a failure band: (a) unconfined response; (b) confined response; (c) resulting yield surface.

In this case, the stress state has two in-plane components (Fig. 18b) and thus results:

$$-\sigma_n = \frac{1}{2} f_{cp}(1 - sin\alpha) - \frac{\sigma_1}{2}\left((1 + sin\alpha) + \frac{1 + sin\varphi}{1 - sin\varphi}\cdot(1 - sin\alpha)\right)$$
$$\tau = \frac{1}{2} f_{cp} cos\alpha - \sigma_1 \frac{sin\varphi cos\alpha}{1 - sin\varphi} \tag{31}$$

That for $\alpha = \varphi$ (to ensure normality to the yield surface, Fig. 8d) it turns:

$$-\sigma_n = \frac{1}{2} f_{cp}(1 - sin\varphi) - \sigma_1(1 + sin\varphi)$$
$$\tau = \frac{1}{2} f_{cp} cos\varphi - \sigma_1 \frac{sin\varphi cos\varphi}{1 - sin\varphi} \tag{32}$$

Both expressions (for the confined and unconfined response) are plotted in Fig. 18c defining the yield surface. The unconfined response corresponds to the arc of circle, with the stress state defined by the angle α. The confined part refers to the straight line, which is tangent and defined by the frictional angle (φ) of the material. In all cases, the normality condition of plastic strain increments is respected (see Fig. 18c).

B.3. Validation of exact solution

The previous solution (Eqs. (29) and (32)) can be claimed to be an exact solution according to limit analysis, as it considers a licit stress field (fulfilling equilibrium and the yield conditions of the materials) compatible with a kinematically-admissible mechanism (refer to Fig. 8a, mechanism whose strain increment field is used for calculation of the stress fields).

An additional check of this condition can be performed by calculating the energy rate balance. For the unconfined regime, the two terms (internal and external energy rates) result:

$$P_e = b{\cdot}t{\cdot}\dot{u}{\cdot}(\tau cos\alpha + \sigma_n sin\alpha)$$
$$P_i = b{\cdot}t{\cdot}\zeta{\cdot}f_{cp}{\cdot}\frac{1}{2}\frac{\dot{u}}{\zeta}(1 - sin\alpha) \tag{33}$$

Leading thus to the condition based on the work rate equation that failure is ensured if:

$$\tau cos\alpha + \sigma_n sin\alpha \geqslant \frac{1}{2} f_{cp}(1 - sin\alpha) \tag{34}$$

Which is fulfilled for every value of α ($\varphi \leq \alpha \leq \pi/2$) by the equations describing the unconfined regime (Eq. (29)).

With respect to the confined regime, the rate of energies result:

$$P_e = b{\cdot}t{\cdot}\dot{u}{\cdot}(\tau cos\varphi + \sigma_n sin\varphi)$$
$$P_i = b{\cdot}t{\cdot}\zeta{\cdot}\left[\left(f_{cp} - \sigma_1\frac{1+sin\varphi}{1-sin\varphi}\right){\cdot}\left(\frac{1}{2}\,\frac{\dot{u}}{\zeta}\,(1-sin\varphi)\right) + (\sigma_1){\cdot}\left(\frac{1}{2}\,\frac{\dot{u}}{\zeta}(1+sin\varphi)\right)\right] \quad (35)$$

Where failure is thus ensured if:

$$\tau cos\varphi + \sigma_n sin\varphi \geqslant \frac{1}{2}\left[f_{cp}{\cdot}(1-sin\varphi)\right] \quad (36)$$

Which is again fulfilled at every point by the equations detailed for the confined response (Eq. (32)).

As a conclusion, it is verified that the proposed solution is exact according to limit analysis, which can be considered as unique accounting for the normality conditions of the plastic strain increments.

References

[1] Cavagnis F, Fernández Ruiz M, Muttoni. An analysis of the shear transfer actions in reinforced concrete members without transverse reinforcement based on refined experimental measurements. Struct Concr, Wiley 2018;19(1):49–64.
[2] Yoon Y-S, Cook WD, Mitchell D. Minimum shear reinforcement in normal, medium, and high-strength concrete beams. ACI Struct J 1996;93(5):576–84.
[3] Cavagnis F, Fernández Ruiz M, Muttoni. Shear failures in reinforced concrete members without transverse reinforcement: a critical analysis on the basis of test results. Eng Struct, Elsevier 2015;103:157–73.
[4] Muttoni A, Fernández Ruiz M. Shear strength of members without transverse reinforcement as function of critical shear crack width. Am Concr Instit, Struct J 2008;105(2):163–72.
[5] Fernández Ruiz M, Muttoni A, Sagaseta J. Shear strength of concrete members without transverse reinforcement: a mechanical approach to consistently account for size and strain effects. Eng Struct, Elsevier 2015;99:360–72.
[6] Zhang JP. Diagonal cracking and shear strength of reinforced concrete beams. Mag Concr Res 1997;49(178):55–65.
[7] Fisker J, Hagsten LG. Mechanical model for the shear capacity of R/C beams without stirrups: a proposal based on limit analysis. Eng Struct 2016;115:220–31.
[8] Classen M. Shear Crack Propagation Theory (SCPT) – The mechanical solution to the riddle of shear in RC members without shear reinforcement. Eng Struct 2020; 210:110207. https://doi.org/10.1016/j.engstruct.2020.110207, 25 p.
[9] Vecchio FJ, Collins MP. The modified compression-field theory for reinforced concrete elements subjected to shear. ACI J 1986;83(2):219–31.
[10] Vecchio FJ. Disturbed stress field model for reinforced concrete: formulation. ASCE, J Struct Eng 2000;126(9):1070–7.
[11] Hars E, Niketic F, Fernández Ruiz M. Response of RC panels accounting for crack development and its interaction with rebars. Mag Concr Res, Thomas Telford Publishing Ltd., London, Vol. 70, No. 8, 2018, pp. 410–432.
[12] Fernández Ruiz M, Muttoni A. On development of suitable stress fields for structural concrete. Am Concr Instit, Struct J 2007;104(4):495–502.
[13] Cavagnis F, Fernández Ruiz M, Muttoni. A mechanical model for failures in shear of members without transverse reinforcement based on development of a critical shear crack. Eng Struct, Elsevier 2018;157:300–15.
[14] Cavagnis F, Simões JT, Fernández Ruiz M, Muttoni A. Shear strength of members without transverse reinforcement based on development of critical shear crack. Am Concr Instit, Struct J 2020;117(1):103–18.
[15] Nielsen MP, Hoang LC. Limit analysis and concrete plasticity. 3rd ed. Boca Raton (USA): CRC Press; 2011788 p..
[16] Jensen BC. Lines of discontinuity for displacements in the theory of plasticity of plain and reinforced concrete. Mag Concr Res 1975;2(2):143–50.
[17] Muttoni A, Fernández Ruiz M, Niketic F. Design versus assessment of concrete structures using stress fields and strut-and-tie models. Am Concr Instit, Struct J 2015;112(5):605–15.
[18] Fernández Ruiz M, Muttoni A. Size effect in shear and punching shear failures of reinforced concrete members without transverse reinforcement: differences between statically determinate members and redundant structures. Struct Concr, Wiley 2018;19(1):65–75.
[19] Muttoni A, Fernández Ruiz M. From experimental evidence to mechanical modelling and design expressions: the Critical Shear Crack Theory for shear design. Struct Concr, Wiley 2019;20:1464–80.
[20] Simões JT, Faria DMV, Fernández Ruiz M, Muttoni A. Strength of reinforced concrete footings without transverse reinforcement according to limit analysis. Eng Struct, Elsevier 2016;112:146–61.
[21] Tirassa M, Fernández Ruiz M, Muttoni A. Influence of cracking and rough surface properties on the transfer of forces in cracked concrete. Eng Struct, Elsevier 225, 111138, 2020, pp. 1—16 https://doi.org/10.1016/j.engstruct.2020.111138.
[22] Sagaseta J, Vollum RL. Influence of aggregate fracture on shear transfer through cracks in reinforced concrete. Mag Concr Res 2011;63(2):119–37.
[23] Xiao J, Sun C, Lange C. Effect of joint interface conditions on shear transfer behavior of recycled aggregate concrete. Constr Build Mater 2016;105:343–55.
[24] Carol I, Prat PC, Lopez CM. Normal/shear cracking model: application to discrete crack analysis. ASCE, J Eng Mech 1997;123(8):765–73.
[25] Carol I, López CM, Roa O. Micromechanical analysis of quasi-brittle materials using fracture-based interface elements, Int J Numer Meth Eng, John Wiley & Sons, Vol. 52, 2001, pp. 193–215.
[26] Cendón Franco DA. Estudio de la fractura en modo mixto de hormigones y morteros, ETSICCP PhD Thesis, Universidad Politécnica de Madrid, 2001, 279 p.
[27] Pundir M, Tirassa M, Fernández Ruiz M, Muttoni A, Anciaux G. Review of fundamental assumptions of the Two-Phase Model for aggregate interlocking in cracked concrete using numerical methods and experimental evidence. Cement Concr Res, Elsevier 2019;125(105855):1–17.
[28] Muttoni A. Die Anwendbarkeit der Plastizitätstheorie in der Bemessung von Stahlbeton, Birkhäuser Verlag, ETH Zürich, No 176, 1990, 164 p.
[29] International Federation for Structural Concrete. *fib* Model Code for Concrete Structures 2010. Germany: Ernst & Sohn; 2013. p. 434.
[30] Moccia F, Kubski X, Fernández Ruiz M, Muttoni A. The influence of casting position and disturbance induced by reinforcement on the structural concrete strength. Struct Concr, Wiley, 2020, pp. 1–28 https://doi.org/10.1002/suco.201900562.
[31] Kim YJ, Sriraman V, Kotwal A, You BH. Confined concrete with variable crack angle – Part II: shear friction model. Mag Concr Res 2014;66(19):967–74.
[32] Magdalena Layos F. On the issue of friction in the analysis of masonry works by means of rigid-body analysis (in Spanish: "El problema del rozamiento en el análisis de estructuras de fábrica mediante modelos de sólidos rígidos"), ETSA PhD Thesis, Universidad Politécnica de Madrid, 2013, 382 p.
[33] Tirassa M. PhD Thesis, École Polytechnique Fédérale de Lausanne; 2020, 238 p.
[34] Jacobsen JS, Olesen JF, Poulsen PN. Constitutive Mixed Mode Behavior of Cracks in Concrete: Experimental Investigations of Material Modeling. Kgs. Lyngby: Technical University of Denmark, 2012, 35 p.
[35] Taylor HPJ. Investigation of the forces carried across cracks in reinforced concrete beams in shear by interlock of aggregate. Cement Concr Res 11, 1970, 22 p.
[36] Hassanzadeh M. Behaviour of fracture process zones in concrete influenced by simultaneously applied normal and shear displacements Division of Building Materials. LTH: Lund University; 1992. p. 105.
[37] Divakar MP, Fafitis A, Shah SP. Constitutive model for shear transfer in cracked concrete, ASCE. J Struct Eng 1987;113(5):1046–62.
[38] Huber T, Huber P, Kollegger J. Influence of aggregate interlock on the shear resistance of reinforced concrete beams without stirrups. Eng Struct 2019;186: 26–42.
[39] Brantschen F, Faria DMV, Fernández Ruiz M, Muttoni A. Bond Behaviour of Straight, Hooked, U-Shaped and Headed Bars in Cracked Concrete}. Struct Concr, Wiley 2016;17(5):799–810.
[40] Calvi PM, Bentz EC, Collins MP. Reversed cyclic experiments on shear stress transfer across cracks in reinforced concrete elements. ACI Struct J 2016;113(4): 851–9.
[41] Fenwick RC, Paulay T. Mechanisms of shear resistance of concrete beams. ASCE, J Struct Division 1968;94(10):2325–50.
[42] Baumann T, Rüsch H. Tests on dowelling action of flexural reinforcement of reinforced concrete beams (in German: Versuche zum studium der Verdübelungswirkung der Biegezugbewehrung eines Stahlbetonbalkens). Deutscher Ausscuss für Stahlbeton 1970;210:42–83.
[43] Hordijk DA. Tensile and tensile fatigue behaviour of concrete, experiments, modelling and analyses, Heron, Vol. 37, No. 1, 1992.
[44] Cladera A, Marí A, Bairán JM, Oller E, Duarte N. The compression chord capacity model for the shear design and assessment of reinforced and prestressed concrete beams. Struct Concr, Wiley 2016;18(2):1017–32.
[45] International Federation for Structural Concrete , fib, Towards a rational understanding of shear in beams and slabs, fib Bulletin Bulletin 85, 2018, 338 p.
[46] Walraven JC. Fundamental analysis of aggregate interlock. ASCE J Struct Eng 1981;107(11):2245–70.
[47] Reza Moradi A, Soltani M, Ali Tasnimi A. Stress transfer behavior of reinforced concrete cracks and interfaces. ACI Struct J 2015;112(1):69–80.
[48] Deng Q, Yi W-J, Tang F-J. Effect of coarse aggregate size on shear behavior of beams without shear reinforcement. ACI Struct J 2017;114(5):1131–42.
[49] Huber P, Huber T, Kollegger J. Investigation of the shear behavior of RC beams on the basis of measured crack kinematics. Eng Struct 2016;113:41–58.